CHAPTER 5

Hysteretic Characteristics in Wood-Frame Structures

One of the major characteristics of wood-frame buildings is their pinching hysteresis. In structural engineering, hysteresis refers to the path-dependence of the structure's restoring force versus deformation. The adjective *pinching* describes the shapes of hysteresis loops in wood-frame structures that appear to be pinched in the middle compared to the hysteresis loops of steel and concrete structures. The physical reasoning behind this behavior is the softening of connection joints. As loading increases in the structure and its connections become deformed, wood fibers are crushed and a nail may begin to yield. If the loading is reversed, the nail moves through the gap formed by the crushed wood fibers. Through each cycle of displacement, depending on the amplitude of the motion, the wood is increasingly indented by the nail. This creates extra spacing where the nail will displace with reduced opposing force (Judd and Fonseca 2005).

This chapter will describe a methodology to extract the hysteretic characteristics of a wood-frame structure from earthquake records. The discrepancies seen in the MODE-ID's predicted responses and the wide range of damping estimates reported in past literature will be discussed as a direct result of the presence of hysteretic response.

5.1 General Concepts

The hysteresis loops of a structure offer vital information about the forces that act upon it and the resulting deformations (Jayakumar 1987; Jayakumar and Beck 1988; Iwan and Peng 1988). It is imperative to accurately map hysteresis curves since they play a pivotal role in creating a better nonlinear model. Fortunately, many of the commercial products that provide nonlinear analyses have the option to input a hysteresis model. The hysteretic behavior of a structure plays a crucial role in many current approaches to seismic performance-based analysis and design. As a result, many experiments have been conducted to record hysteretic data for wood shear walls and other subassemblies. An example illustrating the pinching behavior is shown in Figure 5.1. Although this test was for a single-nail connection, similar behavior is observed for wall and diaphragm components and also for entire structures.

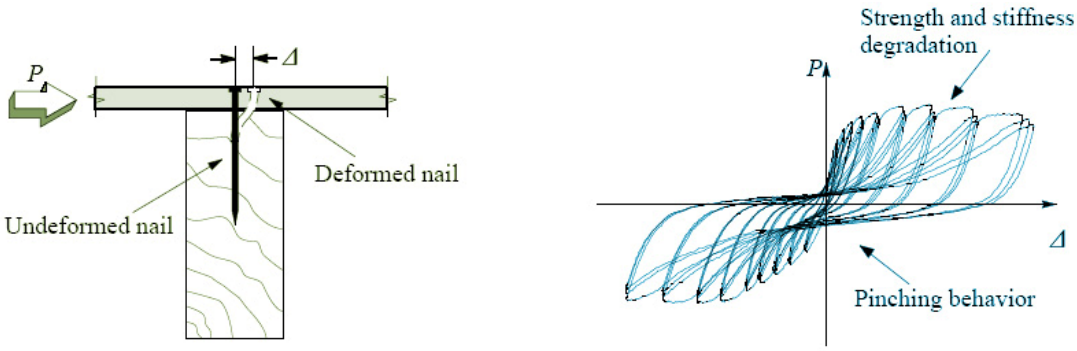

Figure 5.1: Illustration of the nailed sheathing connection and pinching hysteresis curve (Judd 2005).

Extraction of hysteretic characteristics of wood-frame building components can lead to an understanding of the structure's degradation and nonlinear response range. The process involves the construction of a hysteresis curve by plotting time history pairs of restoring force across the component (on the vertical axis), and relative displacement across the component (on the horizontal axis).

Hysteretic behavior has been observed and studied extensively in wooden shear walls. Fischer et al. (2001) conducted a full-scale test structure laboratory experiment and used a nonlinear dynamic time history analysis program RUAUMOKO (Carr 1998) and wood shearwalls program CASHEW (Folz and Filiatrault 2000) to create numerical models. Many hysteresis models have been developed to predict the seismic response of wood-frame structures. Some hysteretic models have produced relatively good results, but the data collected have usually been supported by displacement histories. Records from an instrumented site, such as California's strong motion stations, only have acceleration time histories. Extraction of hysteresis parameters becomes more challenging in the absence of displacement time histories.

5.2 Extraction Process

In theory, velocity and displacement time histories can be obtained directly from an acceleration time history by numerical integration (Iwan, Moser and Peng 1984). It is generally assumed that the calculated velocity and displacement time histories that come with the processed acceleration records contain identical information through numerical integration. However, in processing ground motion histories, additional corrections are

applied to the integrated records which are not reflected in the acceleration histories (Malhotra 2001). It is important to identify these changes if the provided displacement histories are used, as it can alter the results of the hysteresis loops.

After obtaining displacement records, the relative displacement time histories can be calculated by taking the difference between a pair of measurement locations. The relative displacement can be plotted with the restoring force to formulate a hysteresis loop. The restoring force time history can be obtained by scaling the acceleration record with a value representing mass. If the objective is to study the shape of the hysteresis loop, it is not imperative that the exact mass value is used. However, this means that the restoring forces are only as accurate as the mass estimate used. Also, this calculated restoring force is only all-inclusive if the point of interest does not experience other loads. Therefore, it is necessary to construct free body diagrams to correctly attribute all forces.

5.2.1 Free Body Diagrams

Consider the simple structure shown in Figure 5.2a as an example, consisting of north, south, east and west walls (N, S, E and W) and a diaphragm (D) with earthquake acceleration records obtained at locations *a*, *b* and *c* in the N-S direction. We wish to plot the hysteretic curve for the east wall. To obtain the restoring (shear) force time history, a free-body diagram (FBD) is needed as shown in Figure 5.2b. The east wall is cut at mid-height and the diaphragm at mid-span as shown, with the cuts extending through the north and south walls. In the N-S direction, the restoring force at the diaphragm cut is set to zero based on an assumption of symmetric response, and the forces on the north and south walls

are taken as zero because they would be out of plane, leaving only the restoring force F_E on the east wall. The N-S equation of motion is shown in Equation 5-1:

$$F_E(t) = m_a \ddot{x}_a + m_c \ddot{x}_c \tag{5-1}$$

where m_a and m_c are tributary masses for the free body at *a* and *c* and $\ddot{x}_a$ and $\ddot{x}_c$ are the recorded accelerations at *a* and *c*, giving $F_E(t)$ directly. The relative displacement $x_{a\text{-}b}(t)$ across the north wall is obtained by subtracting the doubly integrated acceleration records at a and b. Pairs of $F_E(t)$ and $x_{a\text{-}b}(t)$ are then plotted.

The situation for the diaphragm is different because the shear force varies substantially along the diaphragm, with the maxima at the ends. The procedure employed here extracts the restoring (shear) force $F_D(t)$ at the quarter point and uses a free body consisting of one quarter of the diaphragm and adjacent pieces of the north and south walls cut at mid-height, as shown in Figure 5.2c. With similar assumptions as those made previously, only $F_D(t)$ is present and is determined from Equation 5-2:

$$F_D(t) = m_c \ddot{x}_c \tag{5-2}$$

The relative displacement in this case is $x_{c\text{-}a}(t)$, obtained by subtracting the doubly integrated acceleration records at *c* and *a*.

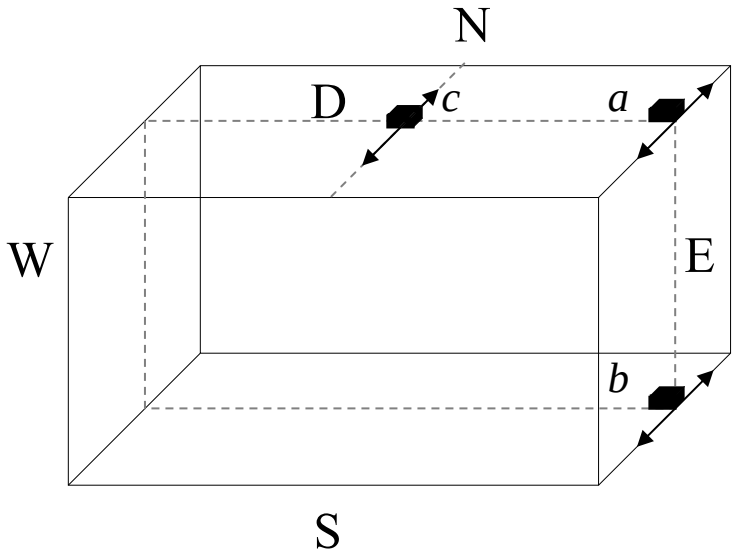

a)

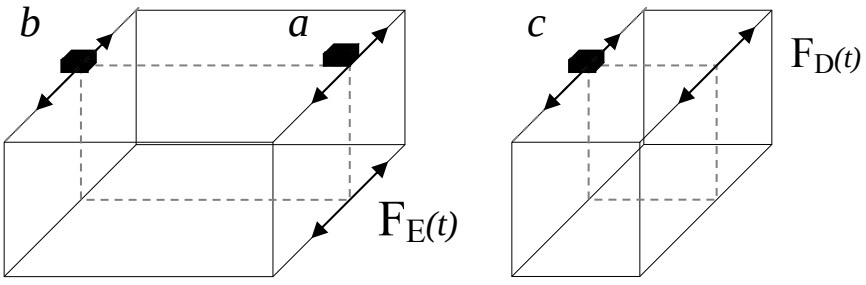

b) **c)**

Figure 5.2: Illustrative example of the free body diagram concept to calculate a hystersis curve.

Using the free body concept described in the previous section, attempts are made to retrieve the hysteretic characteristics of the Parkfield school building. Results are shown in Figure 5.3 (east wall), Figure 5.4 (diaphragm), Figure 5.5 (south wall), and Figure 5.6 (only the shear wall portion of south wall). For example, calculations performed for the hysteresis curve in Figure 5.3 are based on Equation 5-1, with the east wall in Figure 5.2a representing the east wall of the Parkfield school. Channels *a*, *b* and *c* in Figure 5.2 represent channels 1, 3 and 2, respectively (see Figure 3.5). Since the ground motion is assumed to be uniform, it does not matter that channel 3 is not located directly under the Parkfield school's east wall. For the masses m_c and m_a in Equation 5-1, artificial values in the ratio of 1.3 to 1.0 are employed. The use of artificial values means that the force scale in Figure 5.3 is meaningless, but the overall shape of the hysteresis curve is not affected, since it depends only on the ratio of m_c to m_a.

The computed hysteresis curves (doubly integrated from acceleration time histories without any processing) in Figure 5.3 and Figure 5.4 show evidence of pinching in the larger excursions, but not nearly as pronounced as that in Figure 5.1, which was obtained from a controlled laboratory experiment. Results for the south wall in Figure 5.5 can be described similarly. Figure 5.6 may need some baseline correction and filtering of the displacement histories to remove long-period errors (Boore 2005).

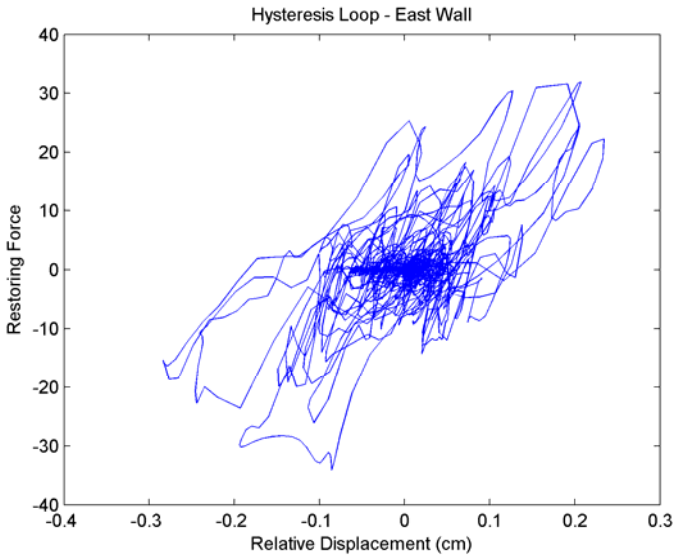

Figure 5.3: Hysteresis curves of the east wall.

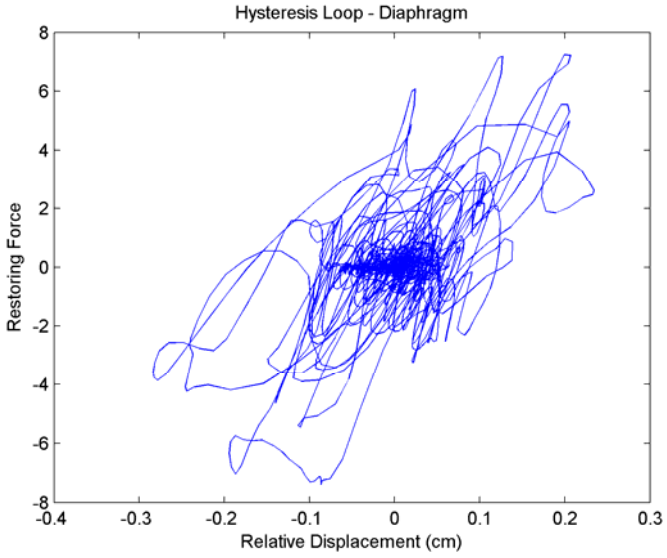

Figure 5.4: Hysteresis curves of the diaphragm.

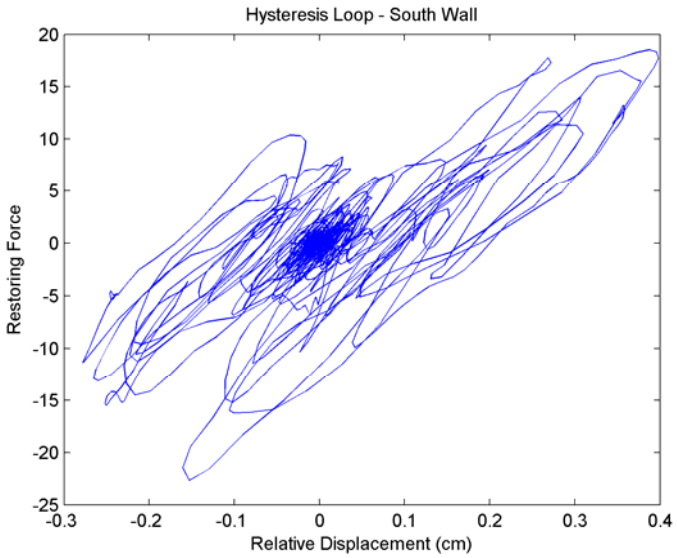

Figure 5.5: Hysteresis curves of the south wall.

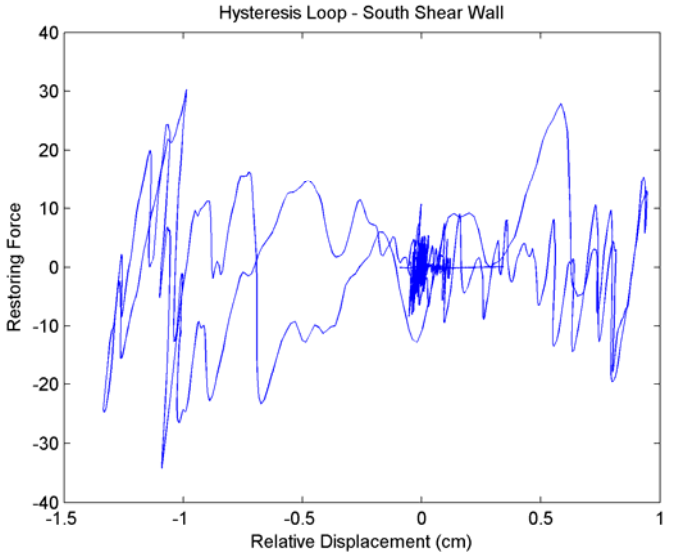

Figure 5.6: Hysteresis curves of the south shear wall.

Compared to hysteresis curves from measured displacement records, the double-integrated hysteresis loops seem chaotic in nature and less meaningful. Laboratory-generated hysteresis loops have experimental setups installed with various sensors. It is evident that obtaining these hysteresis curves would be the most ideal (Graves 2004). When sufficient instrumentation is not available, the practice of the double-integrated acceleration record becomes necessary. The application has served in various capacities such as nonlinear system identification of structures (Cifuentes and Iwan 1989), system identification of degrading structures (Iwan and Cifuentes 1986), and identification for hysteretic structures (Peng and Iwan 1992). However, all of its applications have either been involved with steel or concrete buildings (Cifuentes 1984), integrated from simulated response records from hysteretic models (Peng 1987), or supported by measured displacement time histories. In its application to steel and concrete structures, hysteresis curves are relatively well behaved. As shown in Figure 5.7, the hysteresis loops are slanted in an evident slope. Elastic responses are depicted through the dense slanted lines through the origin. The rotation and expansion of the curves with respect to the origin signify the stiffness reduction and degradation of the structure. This can be a result of yielding, cracking or other forms of failure in structural members (Cifuentes 1984).

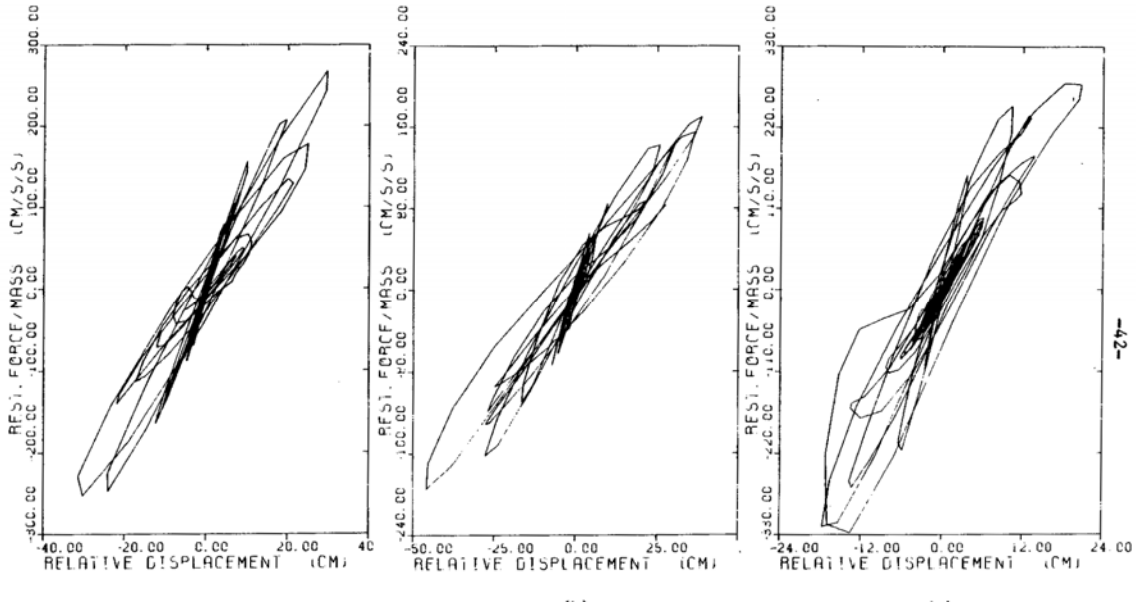

Figure 5.7: Corrected hysteresis curves of non wood-frame structures (Cifuentes 1984).

The same observations cannot be drawn for wood-frame structures. The pinching hysteresis alters the generally elliptical hysteresis loops. With the addition of the high dissipation of energy inherent in wood-frame structures, the area inside the curve fluctuates greatly. Stiffness reduction, unlike steel and concrete buildings, is more apparent in wood-frame structures due to the crushing of wood fibers and may not have a direct correlation to significant structural damages. Therefore, it is important to investigate the applicability of double integrating acceleration records from wood-frame structures, where the pinching hysteresis and high dissipation of energy must be captured. A lot of the complications in accurately mapping a hysteresis curve stem from the lack of measured displacement records. Double-integration errors may be more significant in wood-frame structures.

5.2.2 Double-Integration Errors

The effects of double-integration errors are widely studied in the strong motion instrumentation community. Subtle effects such as tilting or random noise in measurements can cause long period drifts in the recorded time history (Graizer 1979; Trifunac and Lee 1973). The magnitude of these effects is debatable, as some question the robustness of correction schemes. While some claim to successfully calibrate for the displacement errors (Thong et al. 2004) and apply the double-integrated acceleration for soil-structure interaction analysis (Yang, Li and Lin 2006), others adamantly believe these errors are unacceptable when the purpose of the measurement is to verify the integrity of engineering structures (Ribeiro, Freire and Castro 1997).

The correction schemes come in a variety of forms. The most typical approach to resolve the long period response is to apply a baseline correction. The adjustment can take the form of a polynomial (Graizer 1979), leveling out the displacement time history, and bandpass filtering (Trifunac and Lee 1973). However, another problem arises -- it eliminates any permanent displacement and simultaneously reduces the magnitude of the dynamic displacement (Iwan, Moser and Peng 1984). To preserve some of these displacement characteristics, a segmented polynomial baseline fit applied to the raw velocity is proposed (Iwan, Moser and Peng 1985). Since the ground velocity physically begins and ends at zero, the polynomial fit applies these constraints to the initial and final segment of the raw velocity. Integrating and differentiating the corrected velocity time history yields the adjusted displacement and acceleration time history (Wang 1996).

The resulting ground motions from the methods previously mentioned are heavily dependent on the choice of processing parameters. Without any independent constraints, these processing techniques are non-unique (Graves 2004), leaving much room for improvement. Suggestions for better techniques include tailoring procedures based on the specific instrumentation used (Chen 1995), using six-component recording measurements (three linear and three rotational) to eliminate drifts from tilting of sensors (Graizer 2005), and employing geodetic measurements of residual displacement to constrain the processing of the recorded motions (Clinton and Heaton 2004). Other measures are taken at a broader level, such as replacing older analog instruments with digital sensors (Boore 2005) or exploring a strong-motion velocity meter over the current strong-motion accelerometer network (Clinton and Heaton 2002).

Given the variety of methods mentioned above, several improvements are made for the hysteresis loops calculated earlier. Prior to any processing, the integrated time histories from CSMIP are nearly identical to self-integrated acceleration records. Figure 5.8 through Figure 5.11 show the changes in hysteresis loops by using processed records. In each figure, the left hysteresis loop is calculated without any processing. The middle hysteresis loop, labeled as Processed 1, uses baseline correction and minimum phase filtering (i.e. butterworth). The right hysteresis loop, labeled as Processed 2, is same as Processed 1 but uses zero-phase filtering. Zero-phase filtering can be accomplished by passing the record through the same minimum phase filter for the second time, but the record is first reversed in the time domain. Reversing the record again achieves zero-phase filtering on the record. The improvements are apparent in comparison to hysteresis curves using Processed 1. This

demonstrates that processing hysteresis curves are very susceptible to phase delays in filtering. Simple bandpass filtering as suggested by Cifuentes (1984) is not sufficient -- the zero-phase filtered hysteresis curves provide much better results.

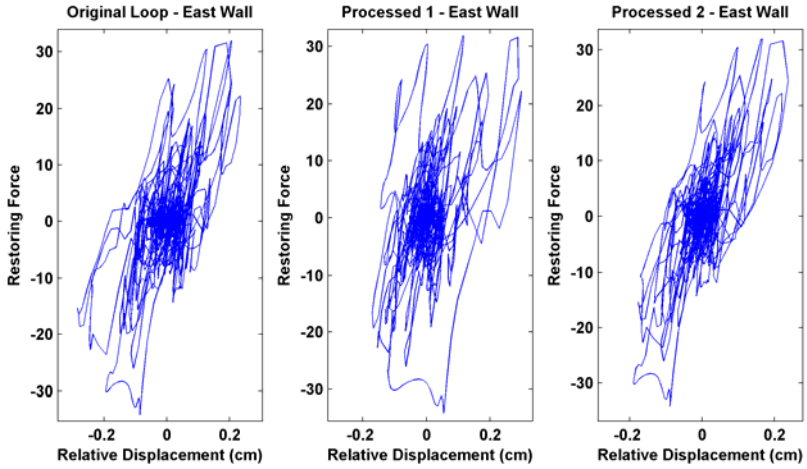

Figure 5.8: Comparison of the pre- and post-processed hysteresis curves from the east wall.

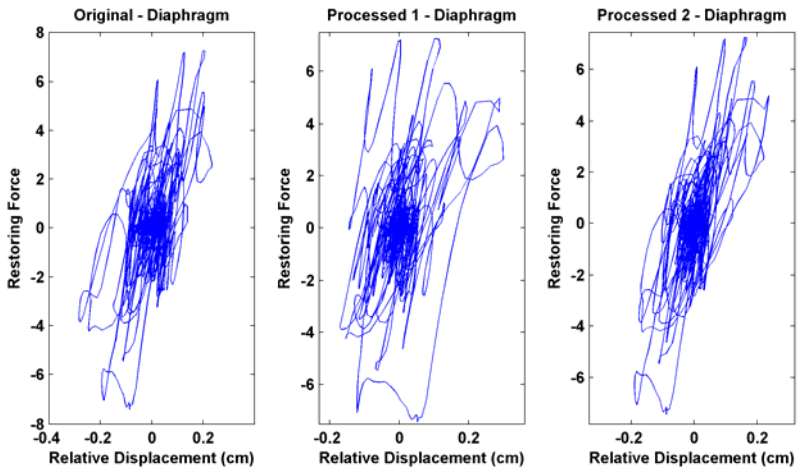

Figure 5.9: Comparison of the pre- and post-processed hysteresis curves from the diaphragm.

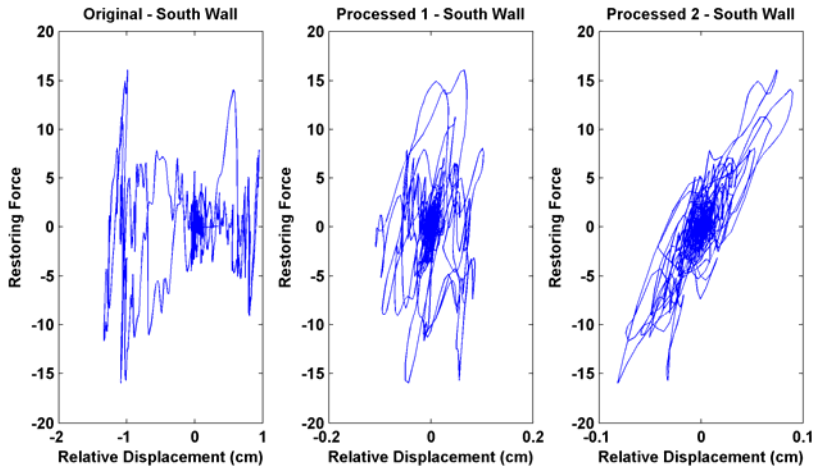

Figure 5.10: Comparison of the pre- and post-processed hysteresis curves from the south wall.

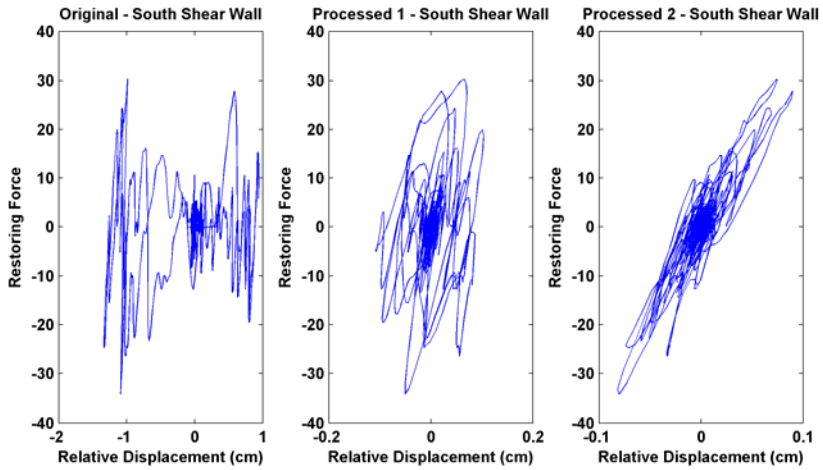

Figure 5.11: Comparison of the pre- and post-processed hysteresis curves from the south shear wall.

The drifts in Figure 5.8 and Figure 5.9 are eliminated and there are signs of slight pinching in each hysteresis loop. Figure 5.10 and Figure 5.11 received the most improvement and suggest mostly linear behavior with slight degradation in stiffness. The use of filters eliminated some of the non-physical behaviors but also tampered with the magnitude of drifts that dictate the shape of the loop. It is hard to verify if some of the pre-processed relative displacement time histories are reasonable. Baseline-fitting corrections are independent for each channel and may complicate the validity of relative displacement time histories. Despite these drawbacks, the extraction of the hysteresis loops have greatly benefitted from the processing. However, an ideal extraction is limited by the instrumentation on site during the event. Therefore, in order to further explore the applicability of double-integrated acceleration in wood-frame structures, the process should first be performed in controlled settings.

5.3 CUREE Task 1.1.1: Shake Table Test - USCD

The shake table tests at UCSD are well instrumented with accelerometers and displacement sensors. Since the tests are performed in a controlled setting, the data recorded are suited for testing the extraction of hysteresis loops through double-integrated accelerations. Figure 5.12 through Figure 5.16 compare hysteresis loops using measured displacements (left) and double-integrated acceleration (right) with different seismic levels. The extracted hysteresis curves from acceleration time histories are good representations of the hysteretic behavior of the structure at all seismic levels. Minor discrepancies are seen on the outskirts of the hysteresis loops at higher seismic levels.

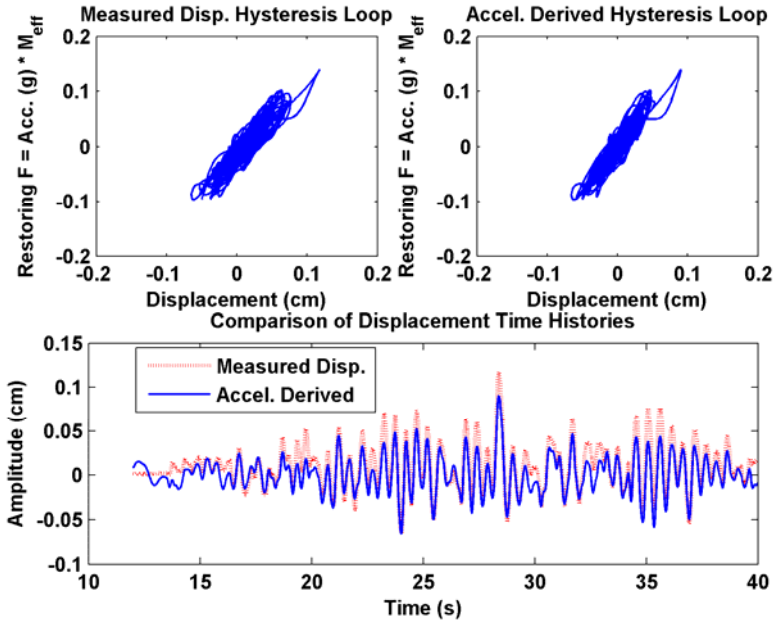

Figure 5.12: Comparison between hysteresis loops derived from measured displacements and double-integrated accelerations. Seismic Level 1 (5% g).

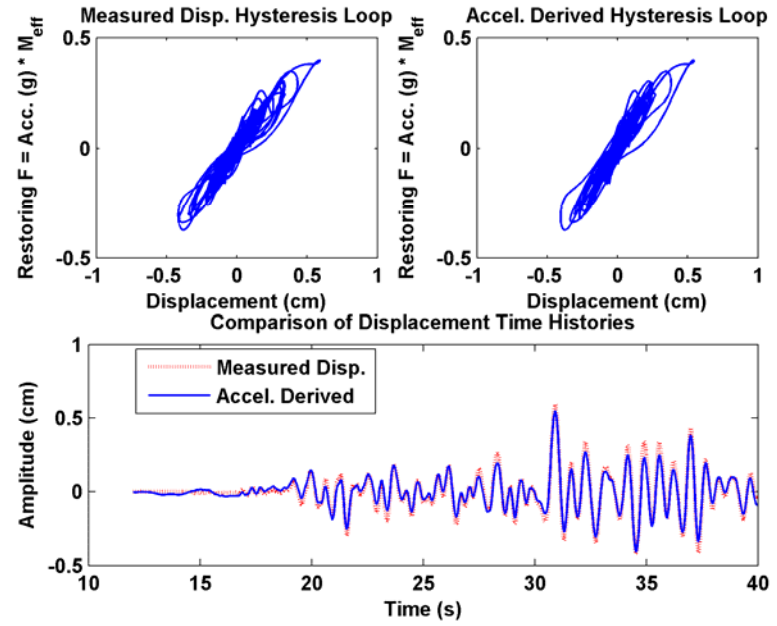

Figure 5.13: Comparison between hysteresis loops derived from measured displacements and double-integrated accelerations. Seismic Level 2 (20% g).

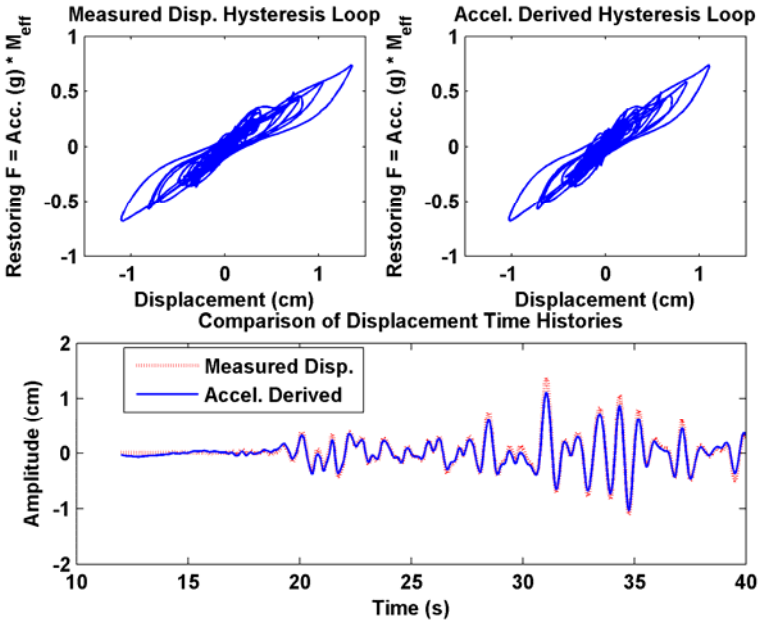

Figure 5.14: Comparison between hysteresis loops derived from measured displacements and double-integrated accelerations. Seismic Level 3 (50% g).

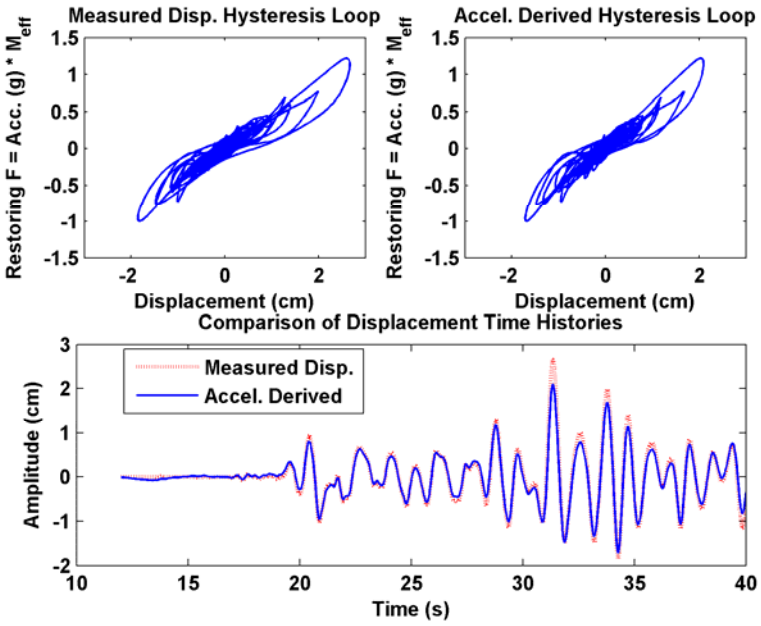

Figure 5.15: Comparison between hysteresis loops derived from measured displacements and double-integrated accelerations. Seismic Level 4 (80% g).

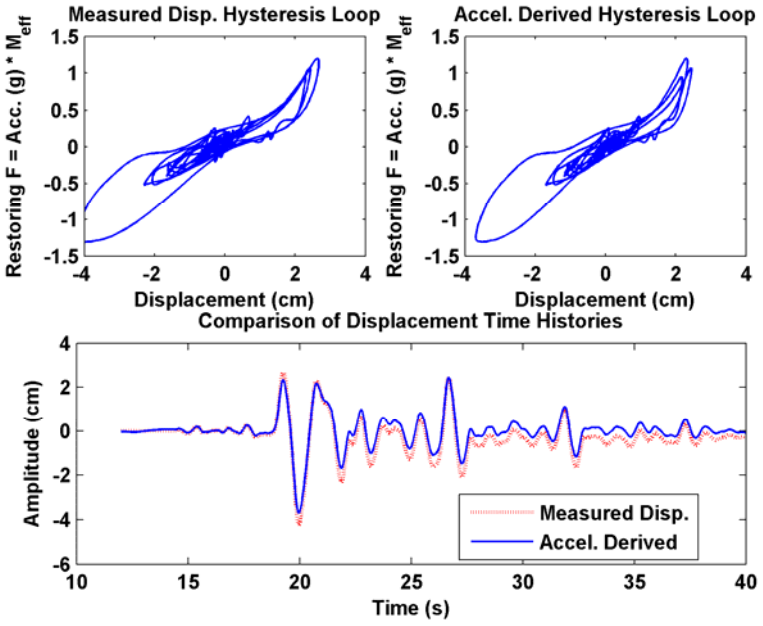

Figure 5.16: Comparison between hysteresis loops derived from measured displacements and double-integrated accelerations. Seismic Level 5 (100% g).

Regardless of these differences, the pinching behavior of the hysteresis loop is clearly represented and captured.

It is interesting that there is such a dramatic difference between hysteretic curves from experimentally obtained data and field records despite applications of the same extraction method. The two records share several common factors: use of a wood-frame structure, same building construction, recording with digitized accelerometers, and similar magnitude of earthquake loading. However, one important note about the experimental test is that the shake table is driven by a uniaxial seismic system. As a result, the building is subjected to forces from a single direction of loading. Unlike in a real earthquake scenario with multi-directional and rotational ground motions, loads perpendicular to the sensors

can cause rotations and tilts that can contaminate the integration process. The ramifications are well described in Graizer (2005).

The contamination is further magnified through the nonlinear behavior of the diaphragm. The multi-directional ground motions can cause nonlinear shearing and therefore introduce forces on the walls that cannot be accurately captured by an uniaxial accelerometer. More importantly, all the behaviors are hysteretic, complicating the extraction process when limited measurements are available.

5.4 Damping

Damping values have always been hard to estimate, the difficulty being that there is no instrument to measure the amount of energy being dissipated. Estimates must be inferred from response data in time or frequency domains. Oftentimes, a linear viscous damping model such as in MODE-ID is assumed for its simplicity and convenience in analysis. This assumption presents two recurring issues in its application to wood-frame buildings:

1) Damping estimates are reported to be much higher than that of steel and concrete structures. Although it is believed that wood-frame buildings dissipate more energy through the friction of joints, it is hard to justify the damping values being several-folds higher.

2) Damping estimates are reported over a wide range of 5% - 20% in wood-frame buildings. These large differences seen among different modal identification

methods and sources of data (seismic response records in the field and dynamic tests in the laboratory) raise questions as to the validity of the reported values.

5.4.1 Compensation for Hysteretic Damping

Many physical systems dissipate energy differently to from viscous damping. Although linear viscous damping is inherent in materials, it may or may not play a significant role in the overall energy dissipation. In wood-frame structures, friction between joints, heat generated from crushing of wood fibers, and nonlinear hysteretic behaviors of structural components, all play an additional role in dissipating energy. It is expected that a linear viscous damping model would have to compensate for these other forms of damping.

Evidence for this compensation can be inferred from both the time and frequency domains. In Chapter 4 it was clear from the windowed analyses that there is a strong amplitude dependence for fundamental frequencies and damping estimates. The variations of the modal parameters in time-segmented records demonstrate the presence of some nonlinear hysteretic response. However, if the analysis is done on a full record, these time-invariant modal parameters, shown in Table 4-1 and Table 4-3, encompass the nonlinearity into single modal parameters that best represent the response.

Another representation can be seen in the frequency domain through the Fourier transform (Brigham 1988; Chopra 2001). Figure 5.17 and Figure 5.18 are the frequency spectrums of the structure with the rigid body motions removed. Losing all time representation, the spectrum shows the signal predominantly in the range of 5 Hz to 8 Hz.

Given the results and conclusions in Chapter 4, we know this multi-peaked frequency band is a result of the shifting of the fundamental frequencies during the seismic ground motion. If a two-mode linear model is meant to characterize this response, the bandwidths of fundamental frequencies must cover the range of 5 Hz to 8 Hz. The nonlinear response inevitably broadens each of the model's resonant peaks. A rough estimate of the damping values can be obtained by the half-power bandwidth (Paz 1997). Estimates can be seen in the 15-20% due to the broadening of the spectrum.

The discussion thus far has been reliant on MODE-ID's time-segmented results that demonstrate the amplitude dependence of modal parameters. The same observations can be made by utilizing other time-frequency representations. A short-time Fourier transform (STFT) can be used to display the frequency content of the signal as it changes over time. The transformation is identical to that of Fourier transform, but a windowing function which slides along the time axis allows for a two-dimensional representation of the signal. Figure 5.19 shows the results of a STFT. A 4-second window is applied to all measurement channels obtained from the Parkfield school building. Each column represents a measurement channel with the changes of the frequency spectrum through time. Starting from the 20-second time interval to the end of record, the vertical axis is adjusted to show the smaller amplitude spectrum. At the first time interval, most of the frequency content is concentrated in the 8 Hz range. During the 4 to 12 second period, which is also when the largest ground motions occur, the spectrum broadens to as low as 5 Hz. The broader spectrum also reaffirms the higher damping estimate seen in the peak of the ground motion.

One drawback of the STFT is the tradeoff between time and frequency resolution. Other time-frequency representations of non-stationary signals such as wavelet transforms (Kijewski and Kareem 2003) and Wigner-Ville (W-V) Distribution (Bradford 2006) are alternatives that yield better temporal and frequency resolutions. Figure 5.20 and Figure 5.21 are W-V spectrums of the Parkfield records. In each figure, the top spectrum is the W-V distribution for the entire record. The bottom spectrum is the W-V distribution with normalized time-segmented records. The reason for the additional time segmentation is that the W-V distribution of the full record is dominated by the largest transient signal in the

ground motion. The analysis will only offer better resolution for the 5 to 10 second period. By applying the W-V distribution in various time segments, the changes in the fundamental frequencies can be better seen. The W-V spectrum has drawbacks such as the introduction of artifacts and negative values (Bradford 2006). Despite these shortcomings, the amplitude dependence of the fundamental frequencies is reaffirmed.

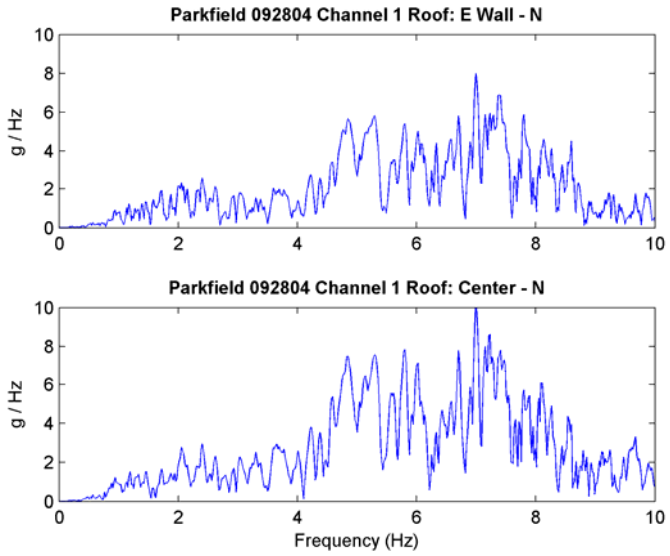

Figure 5.17: Fourier transform of the acceleration time histories from the east wall and diaphragm.

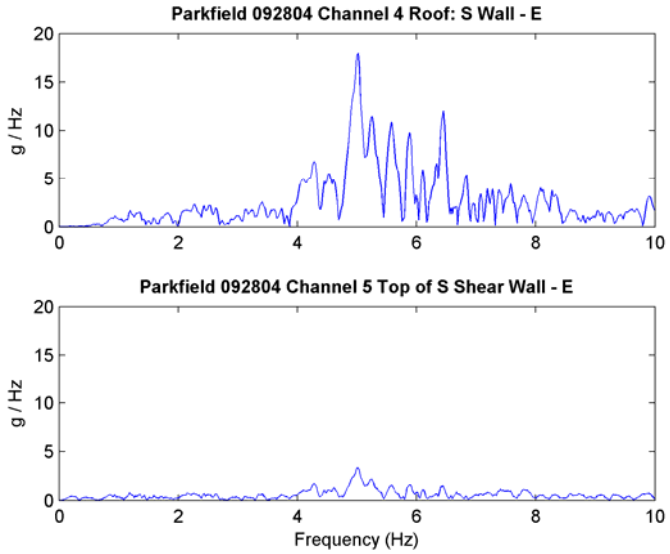

Figure 5.18: Fourier transform of the acceleration time histories from the south wall and south shear wall.

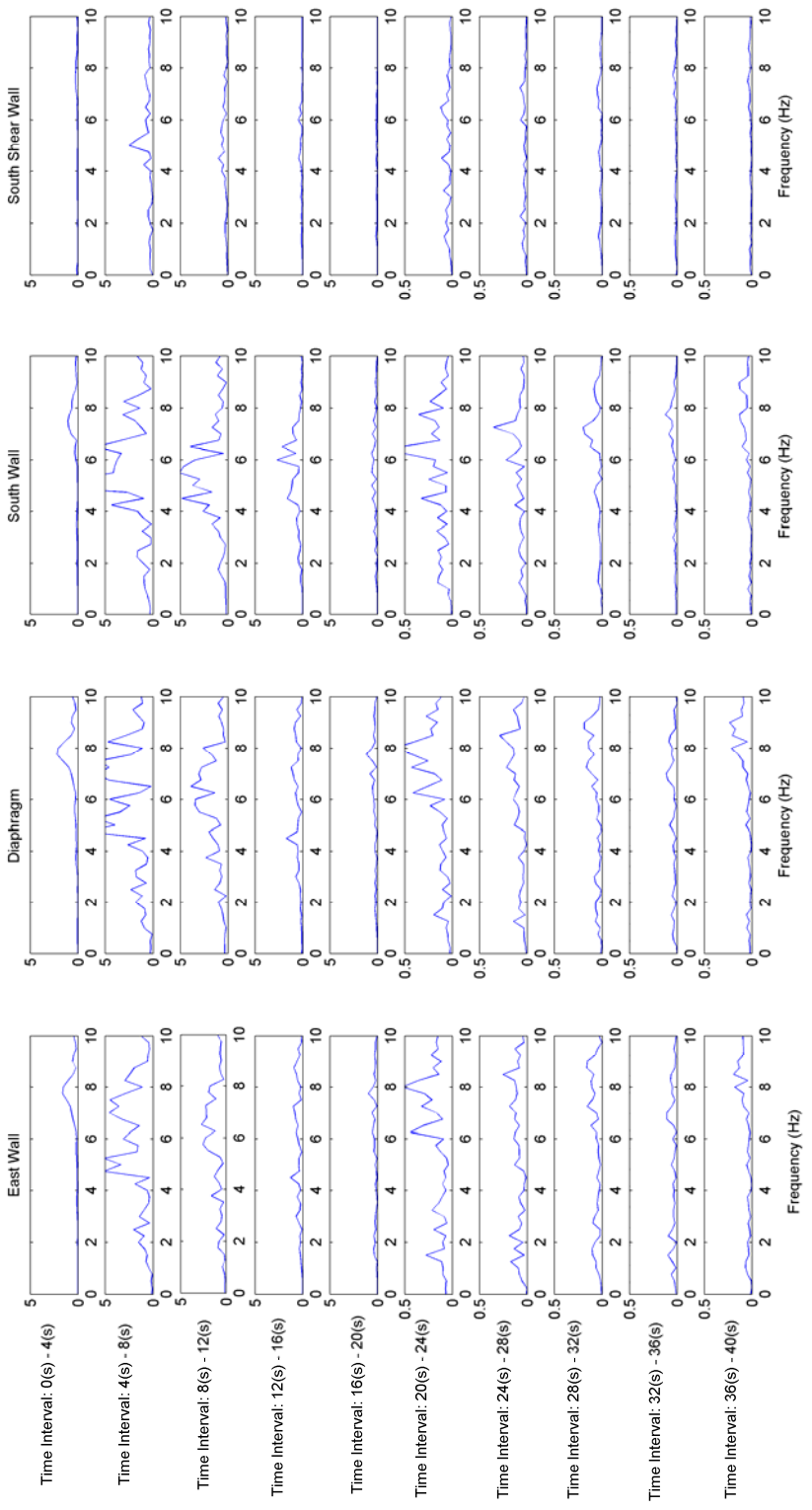

Figure 5.19: STFT of the Parkfield school building with 4 second time intervals.

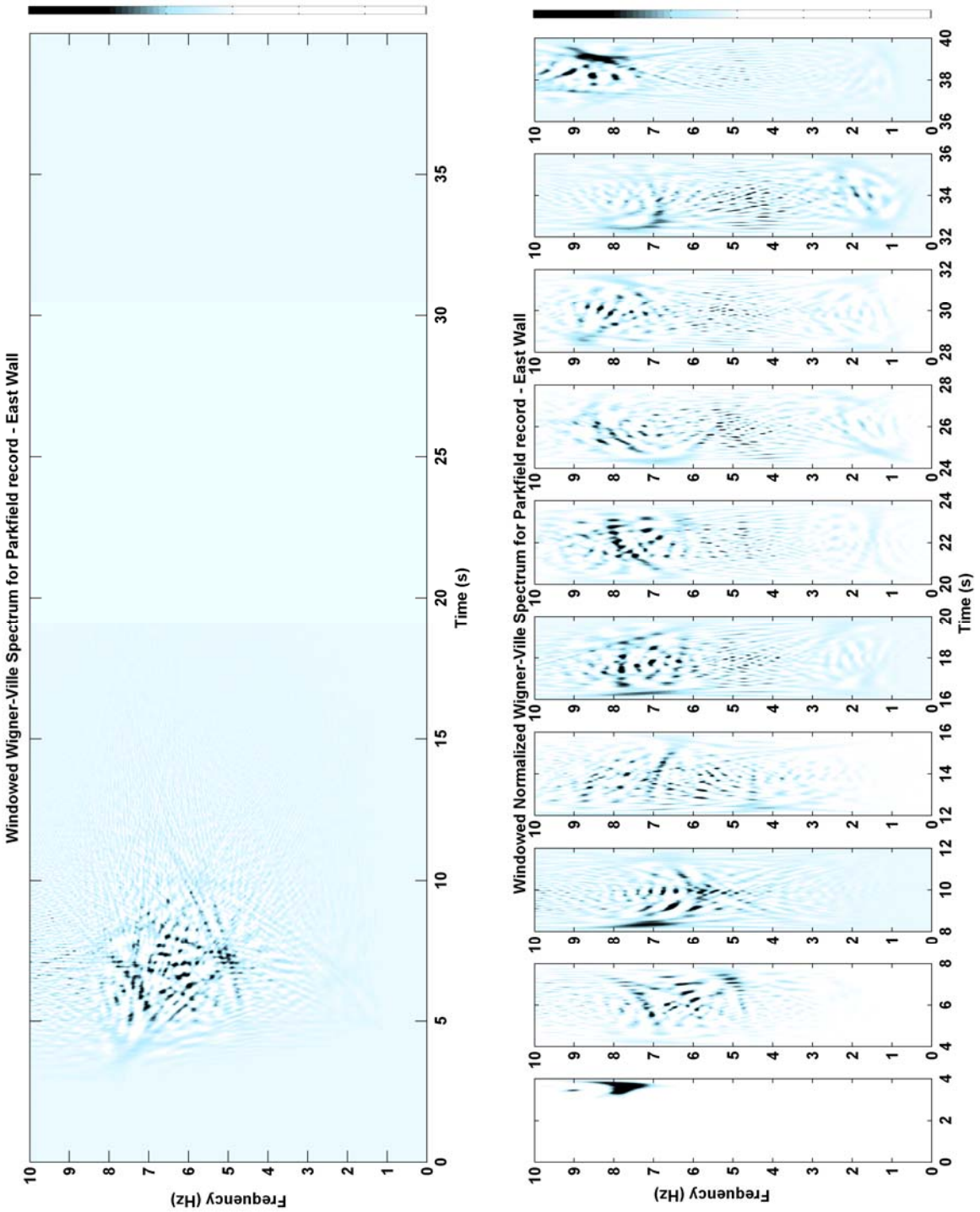

Figure 5.20: Wigner-Ville spectrums of the east wall.

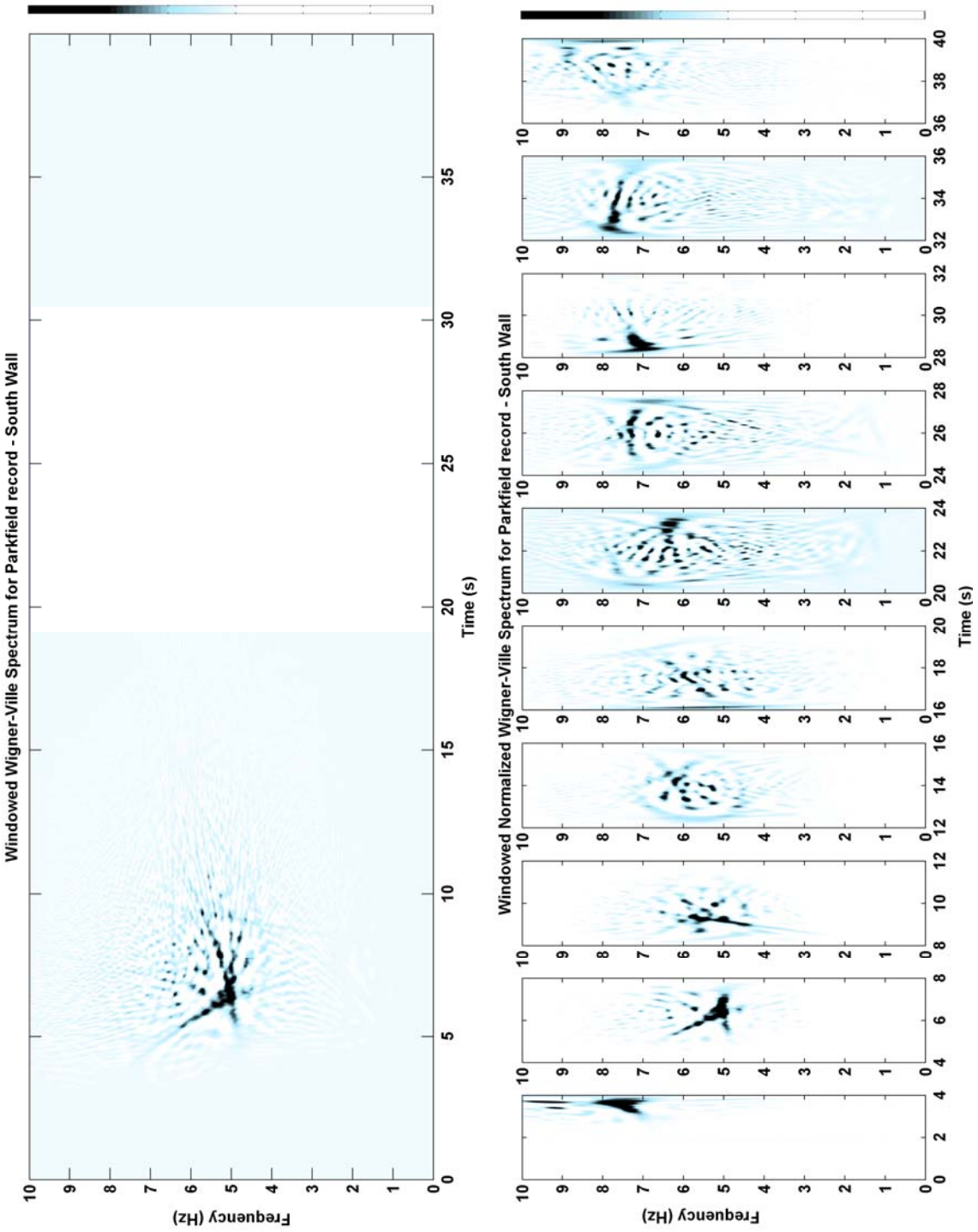

Figure 5.21: Wigner-Ville spectrums of the south wall.

The time and frequency analyses demonstrated that linear modal parameters must compensate for the nonlinear responses. Nonlinearity is introduced by the hysteretic characteristics of the structure. Observations of the hysteresis loops offer several insights to the high damping as well. It is well known that the area inside the hysteresis curve has a direct relationship with the damping estimate (e.g. Uang and Bertero 1986). A formula for calculating the value is available for the linear viscous damper (Paz 1997). An empirical formula for estimating the damping value for nonlinear responses depends on the overall shape of the hysteresis. Even without an exact measurement, the variation in the area enclosed by the hysteresis curve supports the amplitude dependence in damping estimates. Typically, with larger ground motions, the structure yields and higher deformations extend the outer excursions of the hysteresis curve. This inherently increases the area enclosed by the curve and suggests greater energy dissipation. Time-segmented hysteresis loops show the enclosed area as a function of the amplitude of ground motion. The variations support the variations of damping estimates seen in windowed analysis. Therefore, the higher degree of nonlinearity seen in hysteresis loops, the higher the energy dissipation. High linear viscous damping estimates are compensating for hysteretic damping. The procedure here also depends on the extraction of meaningful hysteresis loops. Double-integration errors can hamper this process.

5.4.2 Inconsistencies in Reported Damping Estimates

5.4.2.1. CUREE Task 1.3.3 – Forced Vibration Tests

There are several confirmations of high linear viscous damping estimations as a result of hysteretic damping compensation. However, recent experimentations on full-scale wood-frame structures reported significantly lower damping values. The discrepancies have supported theories that the damping estimates calculated from the MODE-ID method are overcompensating for the hysteretic behaviors in wood-frame structures. The wide range of reported damping values makes it difficult for engineers to determine the appropriate amount of viscous damping to be employed in modeling. Since the choice of damping estimates depends on the type of model being used (linear or nonlinear), it is imperative that scholars emphasize the methods used to calculate the value and describe what the damping estimate represents. Some engineers proclaim that damping estimates over 10% is unreasonable. These statements could cloud the judgment in determining an appropriate damping estimate. One must first recognize that there is no single correct value for damping estimate, as it depends on type of model being used. To further resolve these uncertainties on damping estimates, the hysteretic extraction procedures mentioned in the previous section can help provide insights to this issue.

Forced vibration tests (Camelo, Beck and Hall 2002) reported damping estimates in the range of 2.5% to 8%. The damping estimates were calculated through a regression analysis on the forced vibration measurements. Figure 5.22 and Figure 5.23 show the forced vibration results from the test on a three-story wood-frame apartment complex.

Damping estimates reported are between 4.6% and 5.1%. With the increasing force generated from the shaker, the fundamental frequency is shifted 0.5 Hz. This shift, however, is fairly small compared to the ones observed from the Parkfield school building. This small frequency change suggests that the nonlinear response may not be significant at all. Figure 5.24 to Figure 5.26 are hysteresis loops extracted from the measured accelerations for the apartment complex. Damping estimates are also calculated based on the enclosed area. The hysteresis loops exhibit no signs of pinching and behave like a linear viscous damping element. The cyclic nature of the forces generated from the shaker produce well-defined hysteresis loops in complete cycles.

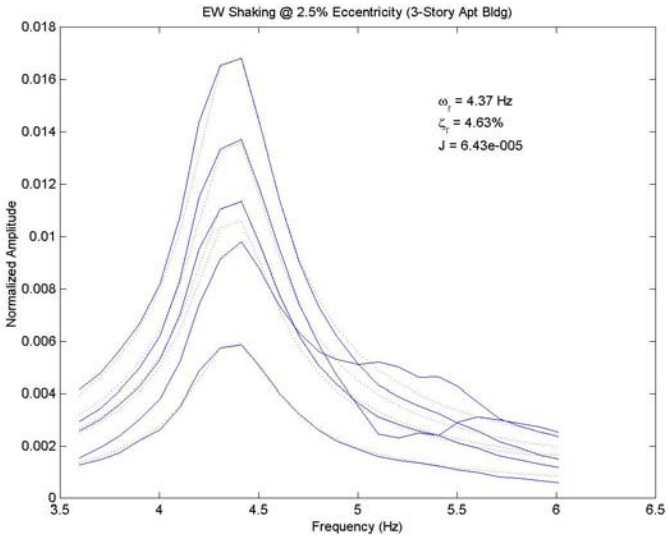

Figure 5.22: Forced vibration results with low level shaking force on the three-Story Del Mar apartment (Camelo 2003).

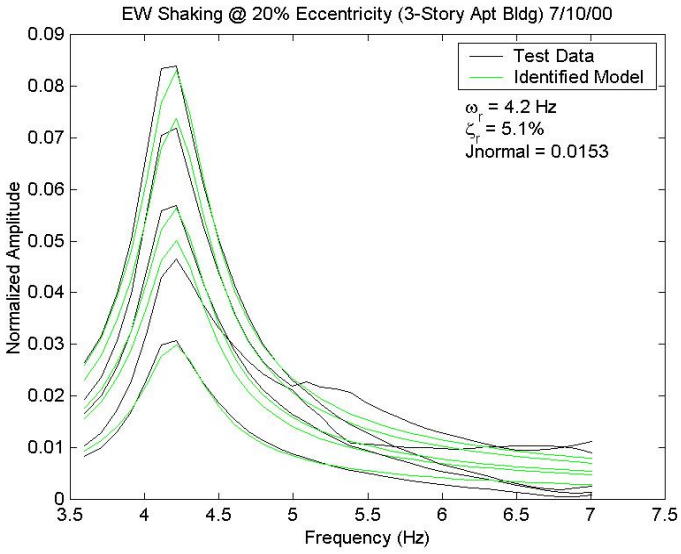

Figure 5.23: Forced vibration results with low level shaking force on the three-Story Del Mar apartment (Camelo 2003).

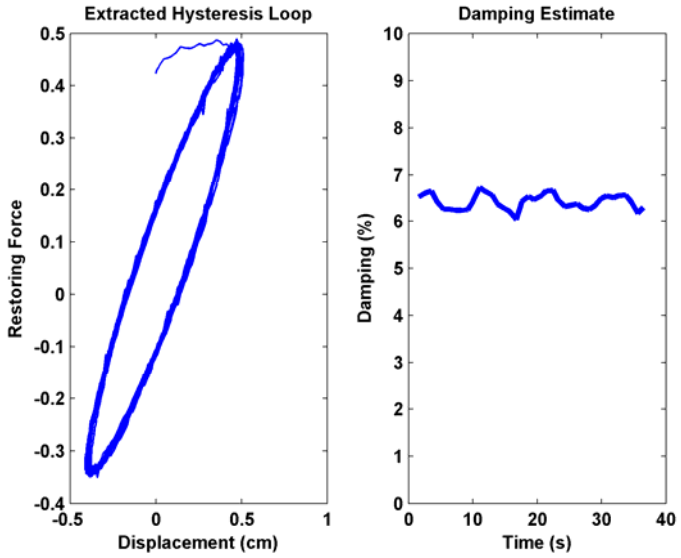

Figure 5.24: Hysteresis loop and damping estimate of the three-story Del Mar apartment building at low level shaking forces.

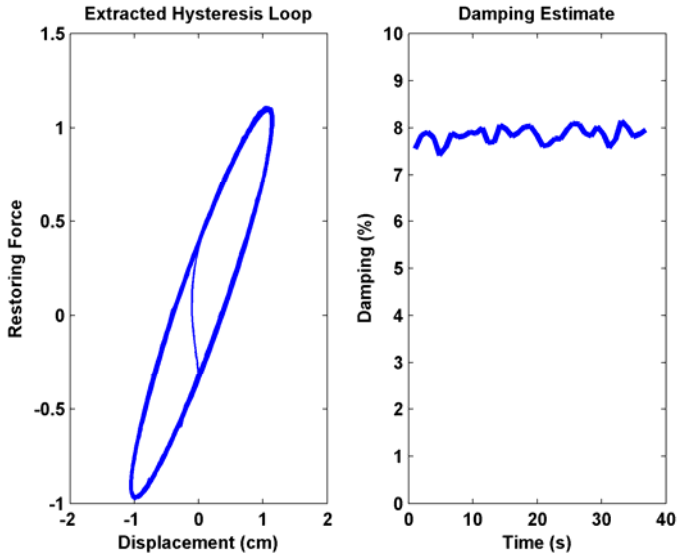

Figure 5.25: Hysteresis loop and damping estimate of the three-story Del Mar apartment building at middle level shaking forces.

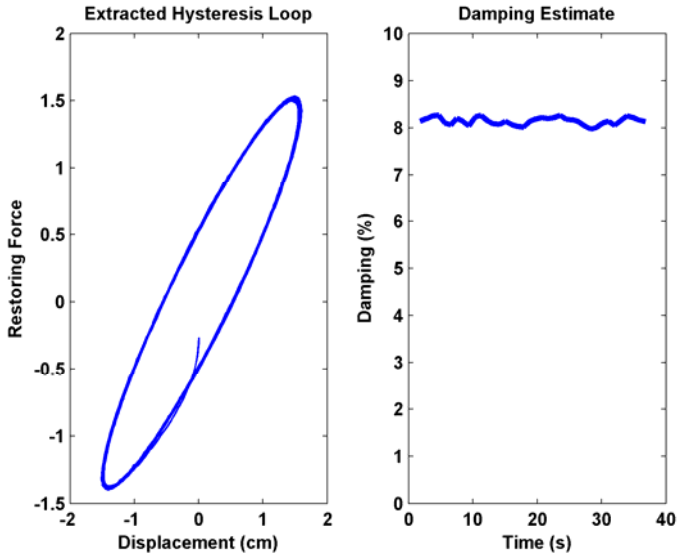

Figure 5.26: Hysteresis loop of the three-story Del Mar apartment building at high level shaking forces.

Since the hysteresis loops has an elliptical shape, we can assume it behaves like a Kelvin solid viscoelastic element. The formula is described in Paz (1997) and Fischer et al. (2001). Calculating the area inside the curve can be done in most numerical packages. The maximum restoring force and relative displacement are also needed for the final damping estimate. The calculations show that the system exhibited 6%-8% damping across increasing forces, which is higher than the 4.5%-5.5% damping estimated by Camelo from fitting resonant peaks. These discrepancies are sensitive to the phase delay and the filter used in the extraction process.

The damping estimation can be applied at multiple time intervals. This may be an alternative way to estimate damping variations with time. Since the shapes of the hysteresis loops suggest little or no nonlinear responses, the method should provide an accurate estimate. However, these forced vibration tests indicated the building's motion exceeded

couple centimeters of vibration. Typically at these amplitudes, the building would show signs of hysteresis. A possible explanation is that forced vibration tests usually record the measurements only during steady state motion. To reach steady state motion, the building experiences shaking levels at constant amplitude for several seconds. At steady state, the building connections may have already softened and measurements may only show the nailed connections traversing the gap created by the initial cycles of the shaking. Therefore, it should be further investigated on the differences of experimental procedures and the impact I has on the results such as showed here for forced vibration experiments.

5.4.2.2. CUREE Task 1.1.1 – Shake Table Tests

The analysis on the series of shake table tests from CUREE Task 1.1.1 report an average damping estimate of 7.6%. Most of the damping values are within one standard deviation (5.3% to 10%). Figure 5.27 compares the modal parameters obtained from the UCSD and MODE-ID analysis. The test specimen is a complete wood-frame structure without sheathing and nonstructural finishes. The ground motions for the seismic tests were scaled versions of the Northridge earthquake, with seismic level 1 having 0.05g peak ground acceleration and level 5 having 0.9g.

The fundamental frequencies match well at lower levels of ground motion, possibly when the structure has not yet reached nonlinear behavior. Amplitude dependence can be seen as these frequency estimates shifted lower during larger seismic motions. The frequencies reported by UCSD were calculated by finding the maximum resonant peak in spectral densities. At higher levels of ground motion where a nonlinear response is

expected, spectral densities are multi-peaked as shown in earlier frequency spectrums. Simply picking the maximum peak in the frequency response will lead to a bias, as seen in the frequency estimates at larger seismic levels.

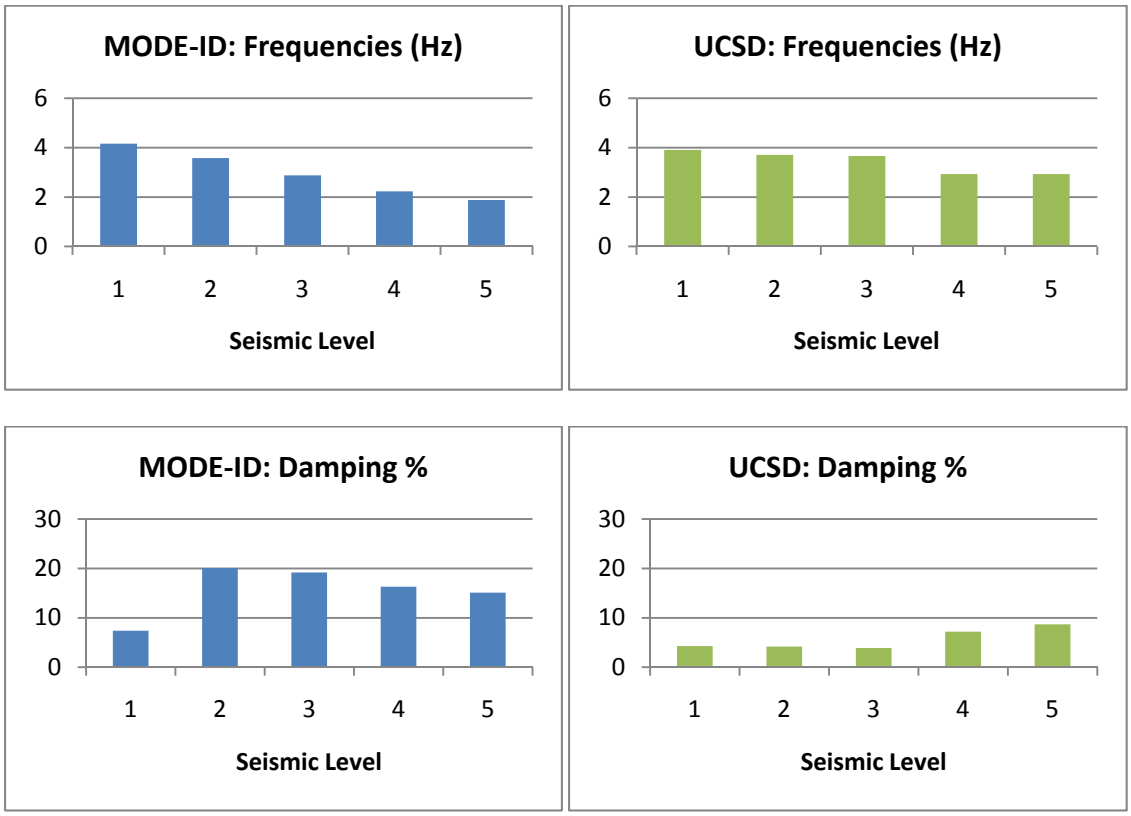

Figure 5.27: Comparison of modal parameter estimates from UCSD and MODE-ID analyses on the same test structure.

By obtaining both the UCSD and MODE-ID analyses and then directly comparing them can lead to very misleading conclusions. One may think that since the fundamental frequencies are similar, comparing the damping estimates can be justified. From Figure

5.27, one might conclude that MODE-ID analysis is inferior, because it reports a 20% damping which can be unreasonable to many structural engineers. However, when comparing these results it is important to understand the methods used to calculate it. MODE-ID analysis uses data fitting based on a linear dynamic model and the modal parameters are the estimates reported in Figure 5.27. The data used were the responses recorded on the test structure during the increasing seismic levels of shaking. On the other hand, the UCSD analysis uses the maximum peaks in frequency domain to conclude these correspond to modal frequencies of a linear dynamic model. The identified frequencies are used to excite the test structure at resonance. The shake table was then brought to a complete stop after the structure had been in resonance for 30 seconds. A logarithmic decrement procedure was used to determine the viscous damping (Fischer, et al. 2001). Although both analyses invoke a linear dynamic model, the MODE-ID calculates an equivalent linear model to strong ground motions and nonlinear responses, while UCSD characterizes the linear behavior of the building after it has experience strong seismic motions. Without properly considering all the differences, reported results of modal parameters can be misleading.

It is true that the UCSD analysis does incorporate the effects of hysteretic damping (Camelo 2003), however, the peak structural acceleration at the roof level for the majority of the tests was only around 0.05g. It is unlikely that nonlinear responses were reached even though the structure was under resonance. Furthermore, most hysteretic behaviors are caused by large deformations and low frequency motions. Shaking the structure at 4 to 6

Hz with a peak structure acceleration of 0.05g typically does not yield the same deformations by large transients as seen in seismic motion.

Additionally, the damping trend for MODE-ID can be supported by understanding the experimental procedures. The same test structure was used for all of the seismic levels. Therefore, if any damage occurred in a previous test, the current test structure is not the same system unless the in-between structural repairs were perfect. If most of the connections were soften during seismic level 2, it is realistic that MODE-ID will report the highest damping value. Later seismic values may have higher amplitudes, but the initial crushing of wood fibers at the connections already happened. .

The damping estimates reported by MODE-ID can be further supported by estimating them from the hysteretic loops obtained from the UCSD building. One way is to first calculate the area inside the pinching hysteresis loop and formulate an ellipse with an equivalent area. The ellipse must have the restoring force and displacement extrema on its perimeter. The damping estimate can then be calculated as previously mentioned.

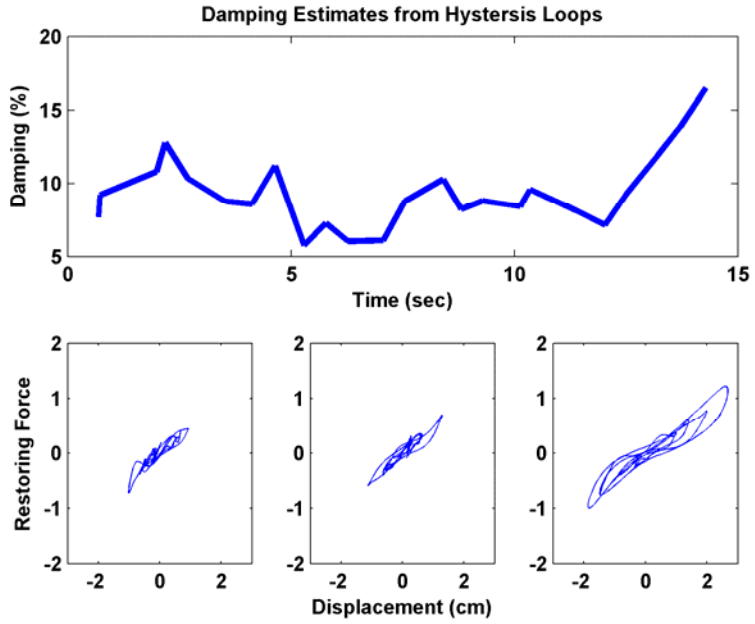

Figure 5.28: Variations in the damping estimate through time. Hysteresis curves are from Test Phase 9 at seismic level 4.

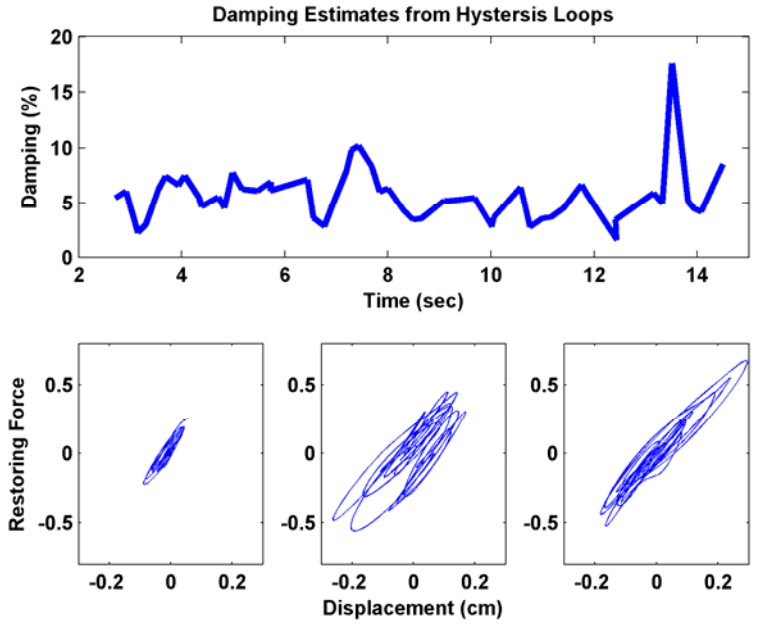

Figure 5.29: Variations in the damping estimate through time. Hysteresis curves are from Test Phase 10 at seismic level 4.

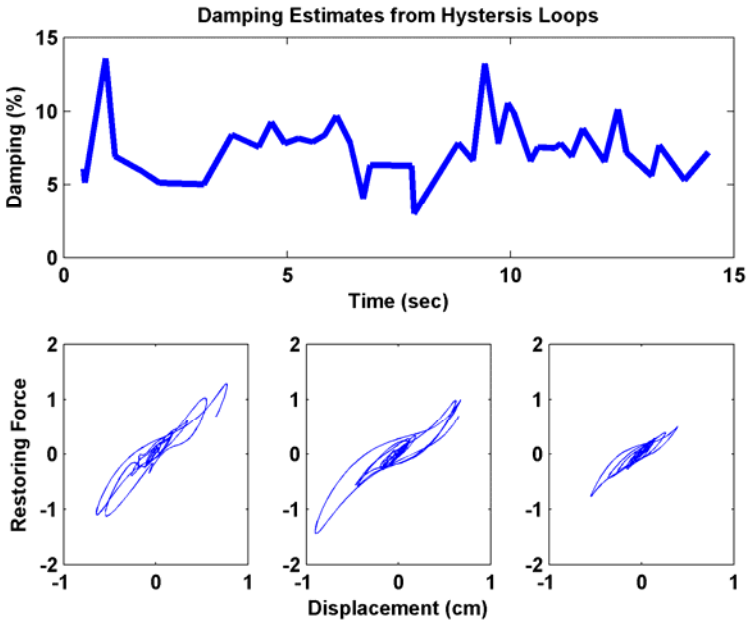

Figure 5.30: Variations in the damping estimate through time. Hysteresis curves are from Test Phase 10 at seismic level 5.

The estimated damping values are consistent with physical intuition. When the pinching hysteresis is more pronounced, the damping estimate is larger. Since the shape of the hysteresis loops changes over time, variations in the damping can occur. Estimating the damping variations through time would require calculating ellipses for each cycle of the hysteresis loop. Figure 5.28 through Figure 5.30 demonstrate how this method can effectively capture the changes in energy dissipation throughout the record. Each figure also provides the hysteresis loops corresponding to the time interval above it. Again, 15% damping are seen when the pinching hysteresis is more prominent.

5.5 Conclusions

Discrepancies seen in the data fitting and reported modal parameters are a result of the hysteretic responses. This chapter has shown that most of the damping estimates reported from MODE-ID are not over-compensating for nonlinear effects. Many of the discrepancies found from experimental results are due to unfair comparisons between linear and nonlinear responses. If a linear model is used to characterize the response, a 12-20% modal damping estimate can be expected for large seismic motion. Nonlinear models with custom hysteresis models should use a 5-10% viscous damping estimate to avoid over-compensating for the dissipation of energy.

This chapter showed that by observing hysteresis loops, one can infer the degree of nonlinearity and the amount of energy dissipated by wood-frame structures. Time-segmented hysteresis curves can yield more accurate estimates in damping fluctuations during seismic motion. These benefits rely on the development of a more robust procedure in extracting hysteresis loops from acceleration measurements. Current procedures are still hampered by double-integration errors and measurement noise. An alternative approach could be to use measured accelerations to identify models with hysteretic elements. This eliminates an intermediate step and avoids double-integration errors.